Volume 22, No 4 | International Journal of Radiation Research, October 2024

Eye lens dose estimations in chest computed tomography examinations using Monte Carlo simulations in a Siemens SOMATOM perspective scanner

M.I. León[1], B. Quispe[1], L. Gutiérrez[2], J.D. Peña[1], G. Waldo[1], P. Cerón[3], M.A. Hernández[2], H.R. Vega[4], E. Montes[1], U. Reyes[5], M. Vallejo[1], M. Sosa[1*]

[1]Department of Physical Engineering, DCI, University of Guanajuato, 37150 Leon, Gto., Mexico
[2]Mexican Institute of Social Security, Health Research Division, High Specialty Medical Unit T1, 37530 Leon, Gto., Mexico
[3]Department of Environmental Sciences, DCIyT, University of Quintana Roo, 77019, Chetumal, QRoo, Mexico
[4]Academic Unit of Nuclear Studies, Autonomous University of Zacatecas, 98000 Zacatecas, Zac., Mexico
[5]State Center of Cancerology, Durango Health Services, 34000 Durango, Dgo., Mexico

► ***Original article***

Corresponding author:
Modesto Sosa, Ph.D.,
E-mail: *modesto@fisica.ugto.mx*

Received: August 2023
Final revised: May 2024
Accepted: June 2024

Int. J. Radiat. Res., October 2024; 22(4): 853-860

DOI: 10.61186/ijrr.22.4.853

Keywords: *Monte Carlo method, eye lens, radiation dosage, tomography.*

ABSTRACT

Background: The radiation dose received by the eye lens when a chest computed tomography (CT) scan is performed, is generally not recorded in clinical practice, particularly due to the distance of this organ from the X-ray beam. ***Material and Methods:*** The absorbed dose in the eye lens was determined by Monte Carlo N-Particle version 5 (MCNP5) calculations and thermoluminescence dosimetry (TLD). Two models of the CT scanner and patient were constructed using the MCNP5 code. The first model was the Bottle Manikin Absorber (BOMAB), which includes the main structures of the eye, and the second was the computational voxelized phantom MAX06. In addition, measurements were carried out in 21 adult patients, which underwent a chest CT study in a Siemens SOMATOM Perspective scanner. ***Results:*** Average Monte Carlo values for the absorbed dose of 16.4 ± 0.4 mGy and 1.97 ± 0.04 mSv for the effective dose were obtained when the BOMAB model was used. Mean values of 13.3 ± 0.3 mGy and 1.59 ± 0.04 mSv, respectively, were obtained for the absorbed dose and effective dose for the MAX06 phantom. TLD measurements gave average values of 12.66 ± 1.33 mGy and 1.52 ± 0.16 mSv for absorbed dose and effective dose, respectively, in simple chest scans, and 7.60 ± 0.63 mGy and 0.91 ± 0.07 mSv, respectively, for simple contrast-enhanced studies. ***Conclusions:*** The results of the Monte Carlo simulations with BOMAB and voxelized phantoms in our study agree relatively well with each other.

INTRODUCTION

Today X-ray imaging-based diagnostic devices are widely used, while their benefits and risks for patients and occupationally exposed personnel have been discussed in many research papers [1-3]. One of the main diagnostic imaging devices are computed tomography (CT) scanners, to produce three-dimensional images of the human body interior. A main task of managing these devices is to avoid ionizing radiation overexposure to the patient because in a CT scan, patients could receive up to 600 times the dose of a conventional radiographic study [4]. Although the X-ray field does not cover all organs in a CT scan, some structures could receive a significant dose from scattered radiation, radiation leaking from the scanner, and background radiation within the room [5]. It is known that the photons used in radiodiagnosis (40 to 150 keV) interact with biological materials, in processes such as the photoelectric effect and Compton scattering [6]. In the first process, total absorption of the photon occurs. However, in the second process the photon is not absorbed and continues its way after undergoing multiple collisions and deviations from its original trajectory, increasing scattered radiation. This radiation can be emitted in any direction and is the principal cause of irradiation in patient's body parts not subjected to examination, it also contributes to the exposure of occupationally exposed personnel and the public [1-3]. Scattered radiation in diagnostic radiology occurs when the primary X-ray beam interacts with the patient, produces a bouncing effect off the body and is scattered in many random directions. In a chest CT scan, the body is exposed to X-rays of 130 kV, which irradiate thin slices (0.6 mm to 1.0 mm), which promote scattered X-ray radiation on the surface of the patient's body and reach other parts of the body that are radiosensitive, such as the thyroid gland, gonads, salivary glands, eye lens and

[DOI: 10.61186/ijrr.22.4.853]

brain.

A huge number of studies dedicated to dose evaluation in radiosensitive organs during CT procedures has been reported in the literature. Several authors have evaluated the dose in the brain, breast and lung in patients undergoing head, chest, and abdomen-pelvis CT examinations [7-15]. One issue presented in these thorax and abdomen-pelvis studies is the absorbed dose in organs far from the irradiation beam, highlighting the lack of information on the eye lens in most of them.

Other interesting studies have focused on evaluating the effect of bismuth shielding on organ dose in CT examinations [7,16-19]. In all cases, a significant reduction of absorbed doses to the breast and thyroid in CT examinations have been reported for exposures with bismuth protection.

On the other hand, according to the International Commission on Radiological Protection (ICRP), the eye lens is one of the most radiosensitive organs, so in 2011 the organization established a dose threshold of 0.5 Gy for chronic exposures, 0.5-2 Gy for acute exposures, and an occupational equivalent dose limit of 20 mSv/year (averaged over 5 years) to prevent the appearance of ocular cataracts [20].

Dose assessment to the eye lens and the risk of eye lens cataract development have been reported in recent studies related to radiation protection in patients undergoing CT procedures of the head [21,22]. Also, dose reduction in eye lens by using bismuth shield in head CT scans have been recently studied [23,24].

However, there is not much information on the risk associated with the eye lens in chest CT procedures. In one of the few recent investigations, Vázquez-Bañuelos *et al*. [25] measured the effective dose in the eye lens in a solid water phantom undergoing a chest CT study, by using the rmoluminescent dosimeters. The authors reported an average effective dose of 57 μSv for the eye lens. For a coronary computed tomography-angiography (CCTA), Shibata *et al*. [26] performed dosimeter determination and computational simulations to estimate the absorbed dose in the eye lens. They found values of 175 mGy and 97.07 mGy, respectively and an average effective dose of 0.1 mSv.

According to this background, there is a lack of information related to the eye lens dose in chest CT procedures. Likewise, the available data show a great variation, so the purpose of this research is to determine the absorbed dose in the eye lens in patients undergoing a CT scan of the chest, using two different methods: Monte Carlo simulation and thermoluminescent dosimetry. The novelty of this work lies in the comparison between computational methods and phantom measurements. Conventional TLD, performed using LiF:Mg,Ti (TLD-100), was employed during this work. On the other hand, a comparison between a BOttle Manikin Absorber (BOMAB) and MAX06 was carried out to assure clinical validation in the results.

MATERIAL AND METHODS

CT scanner

A Siemens SOMATOM Perspective multislice scanner was used for both termoluminescent measurements and Monte Carlo simulations. A total of 21 patients (Mexicans, both genders, aged between 18 and 65 years old) were enrolled in this tomographic study, following the specifications: Gantry aperture of 70 cm, distance from the focus of the X-ray tube to the isocenter of 53.5 cm, power of the X-ray tube from 80 to 130 kVp. The protocol followed consisted of two stages: in the first stage, a general topogram was performed, which allowed determining the exploration area, which in the case of chest exam had a length of 30 cm on average and a width that depended on each patient. In the second stage, the helical exploration was performed in the cranio-caudal direction, following the exploration protocol: cathode-anode voltage of 130 kVp, operating current of 70 mAs, X-ray tube rotation time of 0.6 s, total time of 5.71 s, cutting thickness of 5 mm and pitch of 1.

Monte Carlo calculations

The code Monte Carlo N-Particle version 5 (MCNP5) [27], which was developed at Los Alamos National Laboratory, was used to estimate the fluence and dose. MCNP is a general-purpose Monte Carlo code for performing the transport of neutrons, photons, and/or electrons in various geometries. MCNP offers many convenient features including a powerful geometry modeling tool and various tallies: surface current and flux, volume flux (track length), point or ring detectors, particle heating, fission heating and pulse height tally for energy deposition.

X-ray source simulation

The technical characteristics reported in the literature were used to model the X-ray tube [28]. The model of the X-ray tube was constructed by means of an input file where the cells and surfaces were defined. The compendium of material composition data for radiation transport models was used to simulate the materials of the X-ray source [29]. The X-ray tube was modeled as a cylinder containing the source of electrons (cathode), the target (anode) and its support. This cylinder was filled with diluted air (approximately empty) to avoid energy loss due to electron collisions, see cell 1 in left figure 1. The target was modeled as a 2 mm thick inclined disk attached to a copper cylinder to dissipate the heat that occurs in interactions; the angle of inclination of the target with respect to the vertical was 17°. A 3 mm thick Al filter was included in the model to represent the inherent and additional equipment

[DOI: 10.61186/ijrr.22.4.853]

filter.

The electron source was modeled as a 0.07 cm radius disk that unidirectionally emits 130 keV electrons, as shown in left figure 1. The distance between the electron source and the target was 10 cm. As in the case of cell 1, to avoid the loss of kinetic energy due to collisions, cell 2 in front of the target was filled with diluted air, all encapsulated inside an outer cylinder (see in right figure 1). Subsequently, the modeled X-ray tube was inserted into an enclosure or barrier which was constructed as a truncated cone filled with atmospheric air.

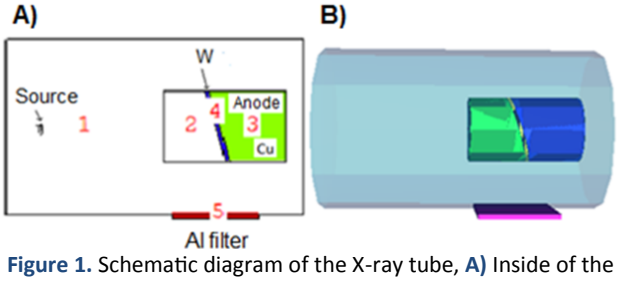

Figure 1. Schematic diagram of the X-ray tube, **A)** Inside of the tube, **B)** 3D view of the tube.

The X-ray spectrum was estimated with the tally F5, which allows to estimate the photon fluence, for each energy, counting the number of photons that cross the detector in terms of photons/cm^2 with a spherical cell filled with air, 3 cm radius, located 50 cm from the focal point for 3 × 10^8 stories.

Patient model

To calculate the doses in eye lens in patients were used two different phantoms, the phantom BOMAB, and the computational voxelized phantom MAX06. The BOMAB phantom simulates an average person 1.70 m tall. This phantom consists of ten cylinders of various shapes (circular and elliptical), whose dimensions are designed to meet the requirements of the reference man described in ICRP 23, with tolerances of ± 10% (Nuclear Technology Services, 2015). The phantom was simulated with the MCNP5 code; the material that was considered for the different parts of the body was equivalent tissue with density 1.04 g/cm^3. Figure 2 shows the different cells considered in the geometry, where the different colors represent the materials. The dimensions of the human eye are approximately constant with variations of 1 or 2 mm between each person. The considerations to simulate the eyeball were: a volume of four concentric spheres with 0.93, 1.03, 1.13 and 1.23 cm of radii, a volume of two concentric sphere represent the cornea and anterior chamber, and the eye lens cell was represented by an ellipsoid with equatorial diameters of 0.8 cm and 0.9 cm, respectively, and a polar radius of 0.25 cm. The mass was considered of 0.20 g, according to the ICRP 23 and 1.07 g/cm^3 density [30]. Using these values, we determined its volume to be 0.1885 cm^3.

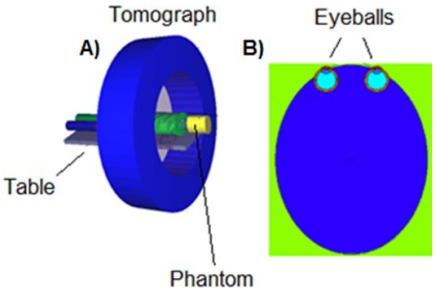

Figure 2. A) Representation of a chest CT on a BOMAB phantom. **B)** Eyeballs placed on the phantom.

A patient table with dimensions of 50×160×5 cm^3 composed of polycarbonate was also simulated. The elemental compositions and densities of different parts of the human eyeball used in these simulations were taken from the work of Asadi *et al.* [31]. The other materials provided by the ICRP and ICRU for phantom and polystyrene-polycarbonate for the patient's table were considered. In left figure 2 the axial axis of the phantom was located at the tomograph isocenter.

The other phantom used was the MAX06, this was built up with 1461 transverse images, each one containing 474×222 pixels, for a total of 153,738,108 voxels of 1.2×1.2×1.2 mm^3. The phantom is described in the work of Kramer *et al.* [32]. The phantom data were processed by Martínez-Ovalle *et al.* [33] for MCNPX syntax to reduce the number of voxels to 3×3×3 mm^3. In this work a phantom with a reduced number of voxels of 271,872 considering the head, thorax and pelvis was used. A voxel size was changed 8×8×8 mm^3. Three tissue compositions and densities: lung, bone, and soft tissue for different organs, similarly for the MIRD5 phantom model were used [34].

To simulate the movement of the X-ray tube around the phantom, the maximum aperture of the tomograph collimators which is 3 cm was used to scan the chest CT. To model the source, a cylindrical shell with an inner radius of 53.499 cm and an external radius of 53.5 cm was considered, thus obtaining a cylinder with a thickness of 0.001 cm and a length of 3 cm, which simulates the opening of the pre-patient collimators. This cylindrical source emits photons from its entire surface into the cylinder, which interact with the thorax of the phantom (see right figure 3). The phantom was located at the tomograph isocenter, with the *yz* plane coinciding with the direction of the longitudinal slice of the phantom and the *xz* plane with the transversal slice.

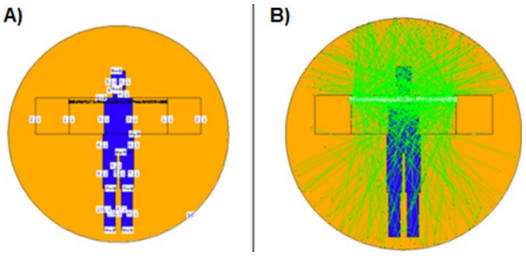

Figure 3. A) Photons emitted from the entire source surface. **B)** Scattered photons due to the interaction with the thorax of the phantom.

[DOI: 10.61186/ijrr.22.4.853]

Fluence and dose estimates

To estimate the fluence in the eye lens the tally F4 was used, which measures the number of photons/cm^2, while the absorbed dose was estimated with tally *F8, which measures energy deposited on a cell in MeV. For conversions to MeV/g values were divided by cell mass, in this case on the cells that represent the eye lens. Also, the number of particles that crossed a surface was determined with tally F1; this measurement was performed on the external surface of the aluminum filter. The estimations were performed using a total of 10^9 stories.

To simulate the helical movement of the scanner, the cylindrical source was modeled considering that it emitted photons from its entire interior surface, thus simulating a 360° movement with continuous shooting in the X-ray tube. The patient's continuous movement was simulated by moving the cylindrical source, generating an input program in MCNP5 for the 30 cm length of exploration of the thorax. In the simulation a pitch equal to 1 was considered.

The absorbed dose (D) in the eye lens and thyroid was estimated according to the equation (1)

$$D=\sum_i^n (Tally*F8)_i \times CF \times NE \times I \times TT \quad (1)$$

where n is the number of cuts, CF is a conversion factor from MeV/g to J/kg, which is 1.6×10^{-10}, NE is the number of electrons/s in 1 mA, given as 6.25×10^{15} electrons/s, I was the operating current (70 mA) of the Siemens SOMATOM Perpective tomograph and TT the total time, 5.71 s. The dose value obtained from equation (1) was multiplied by the fluence of photons produced by an electron that hits the target of the tube, which was 4.87×10^{-4}.

It is known that equation (1) overestimates the dose calculations since this expression does not consider several variables such as the patient or phantom geometry. To scale and validate the Monte Carlo model several measurements of Computed tomography dose index (CTDI) according to the Report of the American Association of Physicists in Medicine (AAPM) Task Group 291 were performed and compared with the Monte Carlo calculations [35].

A 32-cm cylindrical phantom was exposed to a helical beam as a chest study, and doses to the center and periphery of the phantom were recorded. The dose in the phantom (CTDIw) is equal to addition of 1/3 CTDI in the center and 2/3 CTDI in the periphery. The CTDIvol is the ratio between CTDIw and pitch. The ratio between measurement of CTDIvol and the quantity calculated by MC was 0.1852746 and it is considered in the dose expression, denoted as f in equation (2).

$$Dose = f * Doses_{mcnp} \quad (2)$$

On the other hand, the effective dose (E) was calculated from the absorbed dose using equation (3) [36].

$$E = w_T\, w_R\, D \quad (3)$$

where W_T is the tissue risk ponderation factor, W_R is the radiation quality factor and D is the absorbed dose. In this work, W_T was considered as 0.12 for eye lens and W_R equals to 1 [37].

TLD MEASUREMENTS

TLD calibration procedure

A set of TLD-100 dosimeters (Thermo Scientific™, USA) where calibrated using a ^{60}Co source (QSA Global, Inc., USA). To conserve the charge-particle equilibrium the dosimeters were placed at a poly methyl methacrylate (PMMA) dosimeter holder. The dosimeters where irradiated on a 10×10 cm field size with a source-to-surface distance (SSD) of 80 cm. To achieve homogeneity and repeatability in the set, the dosimeters were irradiated with a 25 mGy dose. A statistical analyze was made to ensure homogeneity and repeatability according to the ISO-12974. The selected dosimeters were irradiated from 5 mGy to 56 mGy with the same field size and SSD to generate the calibration curve.

Figure 4 shows the calibration curve for a set of 10 TLD-100 dosimeters. The experimental data (points) were fitted to a linear regression (solid line); a good correlation coefficient (R^2 = 0.977) was obtained. In equation (4) is shown the calibration function obtained from the fit, where D is the absorbed dose in mGy and R_{TLD} corresponds to the response of the TLD-100 dosimeters in nC.

$$D = \frac{R_{TLD}}{0.5133} - 3.9687 \quad (4)$$

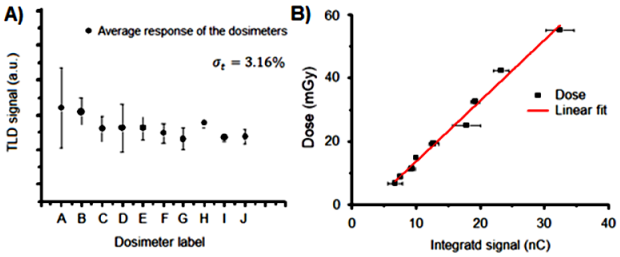

Figure 4. Calibration curve for a set of 10 TLD-100 dosimeters. **A)** Results of the homogeneity test for the TLD-100 batch. **B)** Experimental results data (points) were fitted to a linear regression (solid line) for the calibration curve.

Design and manufacture of the dosimeter holder

A dosimeter holder was designed using acrylic safety glasses. The holes were made at 3.0 mm depth, corresponding to the average depth of the anterior chamber into the eye [37]. The materials of the glasses allow to achieve the charged-particle equilibrium. Each dosimeter holder has a pair of calibrated TLD-100 thermoluminescent dosimeters to measure the absorbed dose in both eyes.

Clinical procedure and absorbed dose measurement

The dosimeter holders were placed on the

[DOI: 10.61186/ijrr.22.4.853]

patients before carrying out their tomographic study. The tomograph used for this study was a Siemens SOMATOM Perspective. Patients were classified according to their type of study (simple, contrast and simple HD). The operation conditions of the equipments were 130 kVp and a range from 75-110 mA according to the autosetup for the patient's weight. After concluding the procedure, the glasses were removed from the patients and placed in especial cases to protect them from other type of radiation.

The clinical CT procedures were performed at the General Regional Hospital of Leon, Mexico. In all cases the medical staff performed the CT scans. No patients or health workers were damage for this research. The study followed the Declaration of Helsinki and written informed consent was obtained from each participant.

Reading and annealing of dosimeters

Twenty-four hours after irradiation, the dosimeters were removed from the glasses and read on a TL reader Harshaw 3500 at a rate of 10 °C/s, with preheating at 50 °C, up to 300 °C. The reading was performed in a nitrogen atmosphere with previous reading of the photomultiplier tube noise and backlight, using the WinREMS software.

After reading, the dosimeters were subjected to a thermal treatment of 1 hour at 400 °C in a muffle and 2 hours at 100 °C in an oven to release and erased the remaining associated tramps. After that thermal treatment, the dosimeters were placed again in their corresponding glasses.

Data and statistical analysis

The acquired data were processed using Microsoft Excel and OriginLab (OriginLab Corporation, USA) softwares. Central tendency and dispersion analyses were conducted utilizing the aforementioned software's, and a p-value test ($p > 0.05$) was performed to validate the statistical data obtained.

RESULTS

Monte Carlo results

Figure 5a shows the beam of electrons emitted by the point source, modeled with the visual editor of MCNPX, the visualization was made for 100 electrons emitted by the cathode. Likewise, in figure 5b the X-ray photons produced in the target for 10,000 particles are observed. As expected, the photons produced in the target are dispersed in a very large cone, and only a few of these travel in the desired direction. This result shows the low efficiency in the production of useful photons in this equipment, which is in good agreement with the expected theoretically [38].

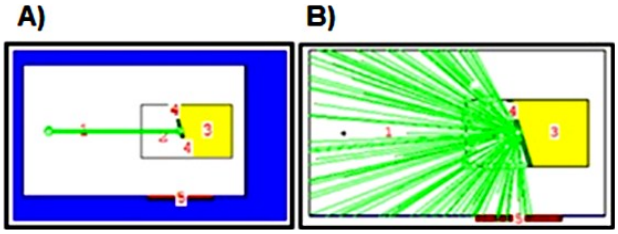

Figure 5. A) Visualization of 100 electrons emitted by the cathode of the point source, modeled with the visual editor of MCNPX. **B)** X-ray photons produced in the target for 10,000 particles.

The simulated X-ray spectrum was made with MCNP5, and it was compared with the theoretical spectrum obtained by SpekCalc [39], with the following characteristics: tungsten target, 130 kVp tube potential, 17° target angle, 3 mm Al filter and 50 cm air distance. Figure 6 shows the comparison of both spectra. It is observed that the spectrum calculated by MCNP5 is in good agreement with the one predicted by SpekCalc, only few differences on intensities (RMS value = 0.042) and the characteristic radiation are observed.

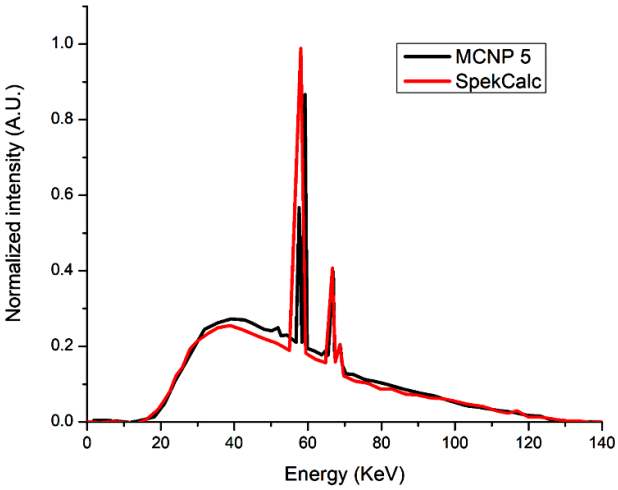

Figure 6. Comparison of spectra calculated by MCNP5 and theoretically by SpekCalc.

To better observe the fluence of the photons through the cells considered in the studied geometry, it was estimated with a mesh tally in the cuts of the eye lens. A cylindrical X-ray source emitting photons from the chest was considered, as can be seen in figure 3 left. Although the X-rays are directed only to the 1st slice of the chest, fluence is seen on the sides of the head, corresponding to photons scattered throughout the patient's chest. A frontal mapping of the fluence is shown in figure 3 right, in a plane approximately at the center of the phantom, where the source emits a ring-shaped X-ray beam. The fluence is greater near the source, as well as in the air -filled space between the phantom and the source. The values obtained from the simulation for the absorbed and effective dose in this study are shown in table 1, for both the BOMAB and the MAX06 phantom. The results of the simulations with the

[DOI: 10.61186/ijrr.22.4.853]

BOMAB phantom were 16.4 ± 0.4 mGy and 1.97 ± 0.04 mSv for the absorbed and effective dose, respectively, while with the MAX06 phantom were 13.3 ± 0.3 mGy and 1.59 ± 0.04 mSv, which correspond to an average absorbed dose in the eye lens of 14.85 mGy and an average effective dose of 1.78 mSv.

Table 1. Absorbed and effective dose in the eye lens obtained in this study, from both from the Monte Carlo simulation and the TLD measurements.

Method	Scanner	CT exam	Absorbed dose (mGy)	Effective dose (mSv)
Measurement results				
TLD measurements (21 patients)	Siemens SOMATOM Perspective	Simple chest	12.66 ± 1.33	1.52 ± 0.16
		Contrast-enhanced simple chest	7.60 ± 0.63	0.91 ± 0.07
Monte Carlo results				
MCNP simulation (BOMAB)	Siemens SOMATOM Perspective	Chest	16.4 ± 0.4	1.97 ± 0.04
MCNP simulation (MAX06)	Siemens SOMATOM Perspective	Chest	13.3 ± 0.3	1.59 ± 0.04

TLD measurement results

The experimental results are summarized in table 1. Two different CT exams were performed, the first was a simple chest CT, while the second was a contrast-enhanced simple chest scan. For a Siemens SOMATOM Perspective scanner, in a study performed in 21 patients, average absorbed doses of 12.66 ± 1.33 mGy and 7.60 ± 0.63 mGy were found for the simple chest and contrast-enhanced simple chest exams, respectively. Effective doses of 1.52 ± 0.16 mSv and 0.91 ± 0.07 mSv were found.

DISCUSSION

A review of the information published in the literature on the eye lens dose for different procedures shows that most of the research works are related to head CT procedures. Alkhorayef *et al.* [21] used the CTDIvol information in 85 patients undergoing a brain CT exam and found an average absorbed dose of 11.5 mGy. Also, Lee *et al.* [8] using a hybrid phantom simulation for a head CT scan reported 13.6 mGy. It is observed that the results reported in these studies are very similar to each other and agree well with the results of our study.

On the other hand, other set of data published in several articles present very discordant results. Jibiri and Adewale [41] found a dose of 35.6 mGy in 26 patients measured using TLD in brain CT scans. Gao *et al.* [14] obtained data in a large sample of 1200 patients in CT brain exams and found doses in the range of 59.9 mGy, while Ngaile and Msaki [42] used the CTDIvol in 500 patients of 8 hospitals and reported 63.9 mGy for the eye lens absorbed dose.

Hence, as it can be observed, the values are spread over a wide range, from 11.5 mGy to 63.9 mGy. One explanation for this difference is that it is due to the difference in parameters such as mA used, as well as the different methods used for estimations. It should be noted that head CT studies were considered in our paper to establish the upper dose limit to calibrate the dosimeters and as a reference to perform the Monte Carlo simulations.

To compare our data with published articles, we consider some recent information available in the literature for the eye lens dose in chest CT procedures. First, there are studies using TLDs, simple geometry phantoms and Monte Carlo calculations [25,43]. These studies show an average absorbed dose of 0.66 mGy for 120 kVp and variable milliamperage (up to 250 mAs). Vázquez-Bañuelos *et al.* [25] employed a TLD measurement on a phantom and reports and absorbed dose of 0.49 mGy, while Alkhorayef *et al.* [43] reports 0.83 mGy. One explanation for the difference between the doses in both procedures is that one of the studies [25] was performed with a conventional CT, while the other was during an angiography [43]. It is important to emphasize that both measurements are much lower than those reported in our study.

On the other hand, a second data set on CT studies published by Shibata *et al.* [26], report absorbed and effective doses in the eye lens in coronary CT angiography. The authors present results from Monte Carlo simulation of 97.07 mGy and 11.75 mSv for absorbed dose and effective dose, respectively, while for patient measurements the results are 175 mGy and 21.19 mSv, respectively. These values are very high compared to other studies. One possible explanation is the high mAs values used in this type of study, up to 600 mAs.

Finally, despite the wide dispersion of published results, all eye lens dose estimates found in the literature, and in our study, are below the 500 mGy threshold for cataract production [44]. Hence, it is clear that when compared to the published articles, our results are in an intermediate range of doses.

The results of the Monte Carlo simulations with BOMAB and voxelized phantoms in our study agree relatively well with each other, yielding an average value for the absorbed dose in the eye lens of 14.85 mGy. For the TLD measurements performed on 21 patients an average value of 10.13 mGy was obtained for the absorbed dose. The data found in our work are part of the few references where the eye lens dose is estimated for chest CT procedures. Our results show that the eye lens received a non-negligible dose in chest CT studies, which suggests that a radiological protection action should be carried out for this organ.

[DOI: 10.61186/ijrr.22.4.853]

ACKNOWLEDGMENT

This work was partially funded by the National Council of Science and Technology (CONACyT), project 257599-CB2020 and by the University of Guanajuato, under the institutional grants for research projects, DAIP-UG 2021. The authors also thank the General Regional Hospital at Leon for the facilities to develop this research.

Ethical Considerations: All subjects gave their informed consent for inclusion before they participated in the study. The study was conducted in accordance with the Declaration of Helsinki, and the protocol was approved by the Ethics Committee of the University of Guanajuato. The study was approved by the Local Health Research Committee 1001 of the Mexican Social Security Institute. Registration CONBIOETICA 11 CEI 003 2018080, dated April 24, 2019.

Funding: National Council of Science and Technology (CONACyT), project 257599-CB2020 and by the University of Guanajuato, under the institutional grants for research projects, DAIP-UG 2021.

Conflicts of interests: The authors declare no conflict of interest.

Author contributions: Conceptualization, M.H., H.V., E.M., U.R., M.V. and M.S.; methodology, M.L., B.Q., L.G., J.D.P., G.W. and P.C.; writing -original draft preparation, B.Q., H.V., P.C. and M.S.; supervision, P.C. and M.S. All authors have read and agreed to the published version of the manuscript.

REFERENCES

1. Chida K (2022) What are useful methods to reduce occupational radiation exposure among radiological medical workers, especially for interventional radiology personnel. *Radiol Phys Technol*, ***15(2):*** *101-115.*
2. Xu XS, Zhang LA, Sun QF, Qin YC, Yu NL (2018) Estimation of the occupational exposure dose for medical diagnostic X-ray workers in Jiangsu, China, using a retrospective dosimetry method. *J Radiat Res,* ***59(2):*** *141-148.*
3. Taqi AH, Faraj KA, Zaynal SA, Hameed AM, Mahmood AAA (2018) Effects of occupational exposure of x-ray on hematological parameters of diagnostic technicians. *Radiat Phys Chem,* ***147:*** *45-52.*
4. Rehani MM and Berry M (2000) Radiation doses in computed tomography: the increasing doses of radiation need to be controlled. *BMJ,* ***320(7235):*** *593-594.*
5. Zira JD, Zikirullahi US, Garba I, Sidi M, Umar M, Bature SS (2020) Assessment of radiation leakage from diagnostic rooms of radiology Department of a Teaching Hospital in Kano, Northwestern Nigeria. *J Nuc Technol Appl Sci,* ***8(1):*** *135-143.*
6. Sato K, Sato C, Takahashi A, Takano H, Kayano S, Ishiguro A, Takane Y, Kaneta T (2022) Accuracy of virtual monochromatic images generated by the decomposition of photoelectric absorption and Compton scatter in dual-energy computed tomography. *Phys Eng Sci Med,* ***45(1):*** *239-249.*
7. Angel E, Yaghmai N, Jude CM, DeMarco JJ, Cagnon CH, Goldin JG, McCollough H, Primak AN, Cody DD, Stevens DM, McNitt-Gray MF (2009) Dose to radiosensitive organs during routine chest CT: effects of tube current modulation. *Am J Roentg,* ***193(5):*** *1340-1345.*
8. Lee C, Kim KP, Long D, Fisher R, Tien C, Simon SL, Bouville A, Bolch WE (2011) Organ doses for reference adult male and female undergoing computed tomography estimated by Monte Carlo simulations. *Med Phys,* ***38(3):*** *1196-1206.*
9. Alonso TC, Mourão AP, Santana PC, da Silva TA (2016) Assessment of breast absorbed doses during thoracic computed tomography scan to evaluate the effectiveness of bismuth shielding. *App Radiat Isot,* ***117:*** *55-57.*
10. Hardy AJ, Bostani M, McMillan K, Zankl M, McCollough C, Cagnon C, McNitt-Gray M (2018) Estimating lung, breast, and effective dose from low-dose lung cancer screening CT exams with tube current modulation across a range of patient sizes. *Med Phys,* ***45 (10):*** *4667-4682.*
11. Yang Y, Zhuo W, Zhao Y, Xie T, Wang C, Liu H (2021) Estimating specific patient organ dose for chest CT examinations with Monte Carlo method. *Appl Sci,* ***11(19):*** *8961.*
12. Tahiri M, Mkimel M, Benameur Y, El Baydaoui R, Mesradi MR, El Rhazouani O (2021) Organ dose estimation for adult chest CT examination using GATE Monte Carlo simulation. *Phys Part Nuclei Lett,* ***18:*** *502-509.*
13. Lee C, Kim KP, Bolch WE, Moroz BE, Folio L (2015) NCICT: a computational solution to estimate organ doses for pediatric and adult patients undergoing CT scans. *J Radiol Protect,* ***35(4):*** *891.*
14. Gao Y, Mahmood U, Liu T, Quinn B, Gollub MJ, Xu XG, Dauer LT (2020) Patient specific organ and effective dose estimates in adult oncology computed tomography. *Am J Roentg,* ***214(4):*** *738.*
15. Akbari-Zadeh H, Seyedi SS, Ganji Z, Sherkat H, Montazerabadi AR, Bahreyni Toosi MT (2024) Pediatric dose references levels estimation for routine computed tomography examinations in Great Khorasan province, Iran**.** ***Int J Radiat Res, 22(1): 179-184*****.**
16. Saba V, Shuraki JK, Valizadeh A, Zahedinia M, Barkhordari M (2020) Reducing absorbed dose to thyroid in neck CT examinations: The effects of Saba shielding. *Radiat Protect Dosim,* ***191(3):*** *349-360.*
17. Ghaznavi H, Momeni Z, Ghaderi S (2021) Assessment of thyroid cancer risk after cervical computed tomography: The impact of bismuth shielding. *Dis Diagnosis,* ***10(2):*** *70-74.*
18. Mehnati P, Malekzadeh R, Divband B, Sooteh MY (2020) Assessment of the effect of nano-composite shield on radiation risk prevention to breast during computed tomography. *Iranian J Radiol,* ***17(1):*** *e96002.*
19. Mourão A, Aburjaile W, Santos SF (2019) Dosimetry and protocol optimization of computed tomography scans using adult chest phantoms. *Int J Radiol Imaging Technol*, ***5(1):*** *1-6.*
20. Yokoyama S, Hamada N, Tsujimura N (2019) Recent discussions toward regulatory implementation of the new occupational equivalent dose limit for the lens of the eye and related studies in Japan. *Int J Radiat Biol,* ***95(8):*** *1103-1112.*
21. Alkhorayef M, Sulieman A, Alonazi B, Alnaaimi M, Alduaij M, Bradley D (2019) Estimation of radiation-induced cataract and cancer risks during routine CT head procedures. *Rad Phys Chem,* ***155:*** *65-68.*
22. Omer H, Alameen S, Mahmoud WE, Sulieman A, Nasir O, Abolaban F (2021) Eye lens and thyroid gland radiation exposure for patients undergoing brain computed tomography examination. *Saudi J Biol Sci,* ***28(1):*** *342-346.*
23. Lee YH, Yang SH, Lin YK, Glickman RD, Chen CY, Chan WP (2020) Eye shielding during head CT scans: dose reduction and image quality evaluation. *Acad Radiol,* ***27(11):*** *1523-1530.*
24. Kawauchi S, Chida K, Hamada Y, Tsuruta W (2022) Lens dose reduction with a bismuth shield in neuro cone-beam computed tomography: an investigation on optimum shield device placement conditions. *Radiol Phys Technol,* ***15:*** *25-36.*
25. Vázquez-Bañuelos J, Campillo-Rivera GE, García-Durán A, Rivera ER, Arteaga MV, Raigosa AB, Vega-Carrillo HR (2019) Doses in eye lens, thyroid, and gonads, due to scattered radiation, during a CT radiodiagnosis study. *App Radiat Isot,* ***147:*** *31-34.*
26. Shibata H, Kondo Y, Fukada S, Asada Y, Kozawa I (2019) Evaluation of radiation dose in coronary computed tomography-angiography examinations: Using organ dose and effective dose. *Radiat Phys Chem,* ***158:*** *218-221.*
27. Brown FB and Nagaya Y (2002) The MCNP5 random number generator (No. LA-UR-02-3782). Los Alamos National Lab. (LANL), Los Alamos, NM, United States.
28. Hayati H, Mesbahi A, Nazarpoor M (2016) Monte Carlo modeling of a conventional X-ray computed tomography scanner for gel dosimetry purposes. *Radiol Phys Technol,* ***9:*** *37-43.*
29. McConn RJ, Gesh CJ, Pagh RT, Rucker RA, Williams IIIR (2011) Compendium of material composition data for radiation transport modeling (No. PNNL-15870 Rev. 1). Pacific Northwest National Lab.(PNNL), Richland, WA, United States.
30. Richmond CR (1985) ICRP publication 23. *Int J Radiat Biol and Related Studies in Phys, Chem Med*, ***48(2):*** *285-285.*

[DOI: 10.61186/ijrr.22.4.853]

31. Asadi S, Vaez-zadeh M, Masoudi SF, Rahmani F, Knaup C, Meigooni AS (2015) Gold nanoparticle-based brachytherapy enhancement in choroidal melanoma using a full Monte Carlo model of the human eye. *J Appl Clin Med Phys,* ***16:*** *344-357.*
32. Kramer R, Khoury HJ, Vieira JW, Lima VJM (2006) MAX06 and FAX06: update of two adult human phantoms for radiation protection dosimetry. *Phys Med Biol,* ***51(14):*** *3331-3346.*
33. Martínez-Ovalle SA, Barquero R, Gómez-Ros JM, Lallena AM (2012) Neutron dosimetry in organs of an adult human phantom using linacs with multileaf collimator in radiotherapy treatments. *Med Phys,* ***39(5):*** *2854-2866.*
34. Akkurt H and Eckerman KF (2007) Development of PIMAL: mathematical phantom with moving arms and legs (No. ORNL/TM-2007/14). Oak Ridge National Lab.(ORNL), Oak Ridge, TN (United States).
35. McCollough CH, Boedeker K, Cody D, Duan X, Flohr T, Halliburton SS, Hsieh J, Layman RR, Pelc NJ (2020) Principles and applications of multienergy CT: Report of AAPM Task Group 291. *Med Phys,* ***47 (7):*** *e881-e912.*
36. Durham J (2006) Concepts, quantities, and dose limits in radiation protection dosimetry. *Radiat Meas,* ***41:*** *S28-S35.*
37. ICRP (2017) Diagnostic reference levels in medical imaging. *Int Comm Radiol Prot Publ,* ***135:*** *Ann. ICRP, 46.*
38. Hashemi H, Heydarian S, Khabazkhoob M, Emamian MH, Yekta A, Fotouhi A (2021) Anterior chamber depth measurement using Pentacam and Biograph in children. *Clin Exp Optom,* ***105(6):*** *582-586.*
39. Haidekker MA (2013) X-ray projection imaging. In Medical Imaging Technology (pp. 13-35). Springer, New York, NY.
40. Poludniowski G, Landry G, Deblois F, Evans PM, Verhaegen F (2009) SpekCalc: a program to calculate photon spectra from tungsten anode x-ray tubes. *Phys Med Biol,* ***54(19):*** *N433.*
41. Jibiri NN and Adewale AA (2014) Estimation of radiation dose to the lens of eyes of patients undergoing cranial computed tomography in a teaching Hospital in Osun state, Nigeria. *Int J Radiat Res,* ***12(1):*** *53-60.*
42. Ngaile JE and Msaki PK (2006) Estimation of patient organ doses from CT examinations in Tanzania. *J Appl Clin Med Phys,* ***7(3):*** *80-94.*
43. Alkhorayef M, Babikir E, Alrushoud A, Al-Mohammed H, Sulieman A (2017) Patient radiation biological risk in computed tomography angiography procedure. *Saudi J Biol Sci,* ***24(2):*** *235-240.*
44. Stewart FA, *et al.* (2012) ICRP publication 118: ICRP statement on tissue reactions and early and late effects of radiation in normal tissues and organs–threshold doses for tissue reactions in a radiation protection context. *Annals of the ICRP,* ***41(1-2):*** *1-322.*

[DOI: 10.61186/ijrr.22.4.853]